

# Anodisation of copper in thiourea-containing acid solution Part II. In situ transversal imaging observations. Kinetics of anodic film growth

A.S.M.A. Haseeb<sup>1</sup>, P.L. Schilardi, A.E. Bolzan, R.C.V. Piatti, R.C. Salvarezza,  
A.J. Arvia\*

*Instituto de Investigaciones Fisicoquímicas Teóricas y Aplicadas — INIFTA — (U.N.L.P., CONICET, CICBsAs), Sucursal 4,  
Casilla de Correo 16, 1900 La Plata, Argentina*

Received 15 April 2000; received in revised form 14 June 2000; accepted 16 June 2000

Dedicated to Roger Parsons with our gratitude after 37 years serving the electrochemical community as Editor of the Journal of  
Electroanalytical Chemistry

## Abstract

The formation of anodic films during the anodisation of copper, at different applied potentials  $E$ , in aqueous 0.5 M sulphuric acid containing different amounts of dissolved thiourea was investigated following the corroding electrode profile by on line in situ imaging. For  $E < 0.07$  V (vs. SCE) the electro-oxidation of thiourea to formamidine disulphide and the electro-dissolution of copper to Cu(I)–thiourea complexes, including the formation of a polymer-like Cu(I)–thiourea complex (film I), take place. For  $E > 0.07$  V, the main reactions are the electro-decomposition of formamidine disulphide and Cu(I)–thiourea complexes yielding a copper sulphide-containing film (film II) and the electro-dissolution of copper as aqueous Cu(II) ions through film II. The relative contribution of these processes depends on thiourea concentration in the solution, the applied electric potential and anodisation time. The growth kinetics of films I and II were determined from the evolution of the average film height  $\langle h \rangle$  obtained from in situ imaging. The kinetics of film I fit a parabolic rate law, whereas those of film II approach a linear  $\langle h \rangle$  versus anodisation time relationship. The rupture of film II assists the localised corrosion of copper. Likely physical mechanisms for the formation of these anodic films are discussed. © 2001 Elsevier Science B.V. All rights reserved.

**Keywords:** Anodic copper dissolution; Thiourea; Corrosion inhibitor

## 1. Introduction

In a previous publication [1] the reactions involved in the electro-dissolution of copper in aqueous thiourea (TU)-containing 0.5 M sulphuric acid and the identification of reaction products at different positive potentials were investigated. This type of information was extremely useful for interpreting the kinetics of those reactions and discussing the most likely physical and chemical mechanisms within a convincing chemical framework.

\* Corresponding author. Tel.: +54-221-4257430; fax: +54-221-4254642.

E-mail address: ajarvia@inifta.unlp.edu.ar (A.J. Arvia).

<sup>1</sup> On leave from Bangladesh University of Engineering and Technology, Dhaka, Bangladesh.

Depending on the concentration of TU ( $c_{TU}$ ), applied potential ( $E$ ), and anodisation time ( $t_a$ ), several reaction products were found. Thus, for the range  $-0.3 \leq E \leq 0.07$  V, the main electrochemical reactions were the electro-oxidation of TU to formamidine disulphide (FDS) and the electro-oxidation of copper to several Cu(I)–TU complex ions [1]. A small amount of these complex ions forms a Cu(I)–TU polymer-like anodic film (film I). The faradic yield ratio of the TU → FDS to Cu(0) → Cu(I) reaction decreases as  $E$  is increased, approaching 1 for  $E \rightarrow 0.07$  V. On the other hand, for  $E > 0.07$  V, the transition of film I to film II occurs within a certain range of  $t_a$  that depends on the solution composition. For  $E > 0.07$  V, the electrodecomposition of FDS and Cu(I)–TU complex ions, accompanied by the electro-dissolution of copper as aqueous Cu(II) ions

results in the formation of insoluble residues on the copper anode (film II). Film II consists mainly of either  $\text{Cu}_2\text{S}$  or a mixture of  $\text{CuS}$  and  $\text{Cu}$ , as concluded from XPS [1].

The present work describes the growth kinetics of film I ( $E < 0.07$  V) and film II ( $E > 0.07$  V). The formation of each one of these films is determined by  $c_{\text{TU}}$ ,  $E$  and  $t_a$ . Kinetic data were obtained utilising a quasi-bidimensional electrochemical cell to follow the outer profile of both the anodic film and the electro-dissolving copper anode by in situ transversal sequential imaging. The use of this technique allowed us to investigate the temporal evolution of the average height ( $\langle h \rangle$ ) of the anodic film and the average depth ( $\langle d \rangle$ ) of the electro-dissolving copper substrate separately. Film I fits a  $\langle h \rangle$  versus  $t_a^{1/2}$  rate law that results from the slow TU diffusion from the solution to the copper anode surface. Conversely, the growth of film II approaches a  $\langle h \rangle \propto t_a$  relationship, which indicates a process most likely governed by the rate of surface electrochemical reactions on copper.

## 2. Experimental

In situ observations of the anodic film growth were carried out using a quasi-bidimensional cell (hereafter referred to as a 2D cell) of a rectangular geometry,  $5.3 \times 3.6 \times 0.02$  cm in size. A scheme of the cell is given in Fig. 1. A strip of electrorefined copper (99.99%, thickness 0.011 cm, exposed length 1 cm) was used as the working electrode, while a platinum strip of similar thickness and an exposed length of 5.3 cm was used as the counter electrode. A saturated calomel electrode acted as the reference electrode. The copper working electrode was polarised at a constant potential set in the range  $-0.1$  to  $2.0$  V (vs. SCE) for values of  $t_a$  up to about 2 h. The diffusion + activation anodic overvoltage ( $\eta_a$ ) was estimated from  $\eta_a = E - IR$ , where  $IR$  is the ohmic drop correction.

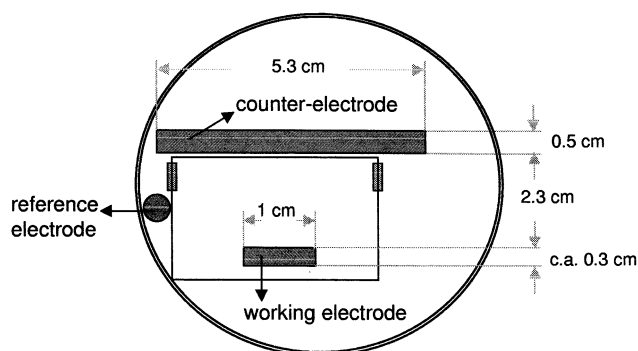


Fig. 1. Scheme (top view) of the 2D cell.

Aqueous 0.5 M sulphuric acid solutions were used varying the concentration of TU in the range  $0.01 \leq c_{\text{TU}} \leq 10$  mM. Plain aqueous 0.5 M sulphuric acid was also used for comparison purposes. Solutions were prepared from TU (Fluka, puriss. p.a.), sulphuric acid (Merck, p.a.) and Milli-Q\* water.

The electrochemical instrumentation consisted of a PAR model 362 scanning potentiostat coupled to a Houston Omnigraphic recorder. The polarisation curves were recorded at a scan rate of  $0.005 \text{ V s}^{-1}$  to approach quasi-steady state polarisation conditions.

During polarisation, the 2D cell was placed under a microscope (Carl Zeiss STEMI 2000C) and the changes occurring at the edge of the working electrode facing the counter electrode were observed using transmitted light. A cold lamp was utilised as a light source. A video camera was employed to transfer and record the images on a computer by means of commercial image processing software (Kontron KS 300 V2).

SEM samples were prepared both in the 2D cell and in a conventional cell using an anode made from an electrorefined copper sheet (exposed area  $0.5 \times 0.7$  cm). The anode was placed horizontally with its exposed area facing up in order to avoid any mechanical dislodgement of the film. SEM data were obtained with model XL30 FEG Philips equipment.

All the measurements were performed at room temperature.

## 3. Results

### 3.1. Polarisation curves

The anodic polarisation curve from copper electro-dissolution as  $\text{Cu}^{2+}$  ions in aqueous 0.5 M sulphuric acid using a conventional three-electrode arrangement 3D cell (Fig. 2, line 1), in which the ohmic overpotential was negligible at least in the potential range  $0.0 \leq \eta_a \leq 0.2$  V, approaches a Tafel relationship  $\eta_a = a_0 + b_T \log j$ , with a slope  $b_T = 0.044 \text{ V decade}^{-1}$  and  $a_0 = 0.21 \text{ V}$  (Fig. 2), in agreement with data reported in the literature [2]. However, for  $\eta_a > 0.16$  V, data deviate from the Tafel relationship due to ohmic and mass transport overvoltage resulting from the local precipitation of copper sulphate.

The same experiment was made using the 2D cell (Fig. 2, line 2). In this case, the anodic polarisation curve involved an ohmic resistance of about  $40 \Omega$  due to the geometric characteristics of the cell. This figure was in agreement with the values of  $R$  estimated from the geometry of the 2D cell, using the experimental conductivity of the solution  $\kappa = 0.175 \text{ mS cm}^{-1}$  at 298 K.

Runs made in the 2D cell for TU-containing solutions showed an additional increase in the value of  $R$

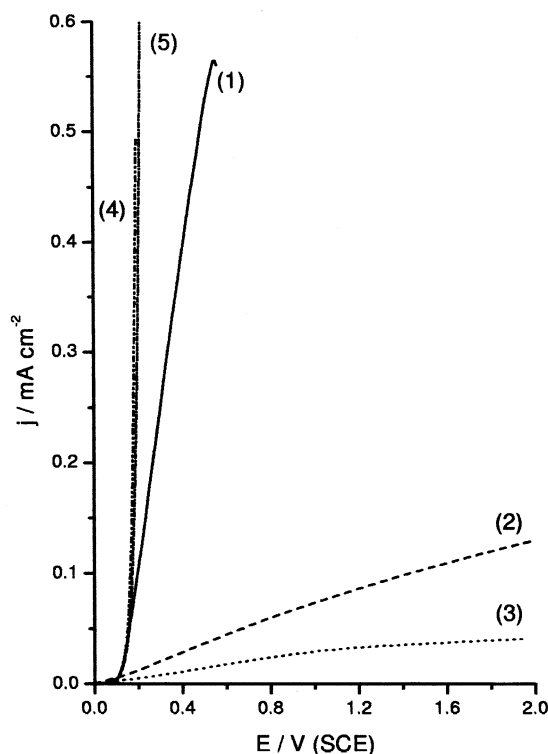


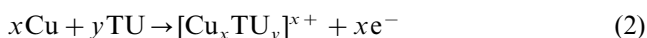
Fig. 2. Anodic polarisation curves for copper electrodisolution run at  $v = 0.005 \text{ V s}^{-1}$ . (1) 0.5 M sulphuric acid using a conventional three-electrode cell. (2) 0.5 M sulphuric acid using the 2D cell. (3) 0.5 mM TU + 0.5 M sulphuric acid using the 2D cell. (4) Theoretical curve resulting from 0.5 M sulphuric acid considering a Tafel relationship with  $b_T = 0.044 \text{ V decade}^{-1}$  and  $a_0 = 0.21 \text{ V}$ . (5) Theoretical curve resulting from 0.5 mM TU + 0.5 M sulphuric acid considering a Tafel relationship with  $b_T = 0.055 \text{ V decade}^{-1}$  and  $a_0 = 0.23 \text{ V}$ . Apparent electrode area  $0.3 \text{ cm}^2$ . 298 K.

within the range  $40 \leq R \leq 56 \Omega$ , depending on  $c_{\text{TU}}$  (Fig. 2, line 3). This increase in the value of  $R$  was due to the blockage of the anode surface by film formation [3,4]. Once the different contributions to  $R$  in the 2D cell were compensated, the anodic polarisation curve in the presence of TU was coincident with the one predicted by a Tafel relationship with  $b_T = 0.055 \text{ V decade}^{-1}$  and  $a_0 = 0.23 \text{ V}$  (Fig. 2, line 5) [1].

For TU-containing solutions, the very initial anodic process is dominated by the electro-oxidation of TU to FDS [1]



and the formation of Cu(I)–TU complex ions that can be expressed by the formal reaction



where  $[\text{Cu}_x\text{TU}_y]^{x+}$  stands for Cu(I)–TU complex ions with  $x < y$  [5].

Conversely, for  $E > 0.07 \text{ V}$ , the electrodisolution of copper proceeds via the global reaction



as demonstrated spectrophotometrically [1]. Reaction (3) is influenced by the presence of the anodic film.

The total anodisation time to record the polarisation curve depicted in Fig. 2, for 0.5 mM TU + 0.5 M sulphuric acid using the 2D cell, was  $t_a \approx 400 \text{ s}$ . Accordingly, the maximum charge passed through the cell resulted in  $12 \times 10^{-3} \text{ A} \times 400 \text{ s} \approx 5 \text{ C}$ . Taking into account the effective volume of the 2D cell,  $V \approx 0.3 \text{ cm}^3$ , the charge required for the full conversion of copper into Cu(I)–TU complexes in the cell was about 15 mC. This figure is much smaller than the maximum charge involved in the polarisation run plotted in Fig. 2. Consequently, data from Fig. 2 are related to reaction (3) as this is the predominant reaction over the whole range of  $t_a$ . The tendency of the polarisation curve to attain an anodic limiting current at high positive potentials can be related to the interference of film II, resulting from the electrodecomposition of TU-containing species, in the overall anodic process.

### 3.2. SEM micrographs

SEM micrographs of anodic films, produced from copper in  $x \text{ mM TU} + 0.5 \text{ M sulphuric acid}$  at different values of  $\eta_a$ ,  $c_{\text{TU}}$  and  $t_a$ , are shown in Figs. 3–5. SEM micrographs were obtained after the samples were first rinsed with water and then air-dried. For  $c_{\text{TU}} = 0.5 \text{ mM}$  and  $\eta_a = 0.04 \text{ V}$  ( $I = 3 \mu\text{A}$ ), the anodic charge associated with the film produced after  $t_a = 8100 \text{ s}$  is 16 mC, a figure close to that expected from either reactions (1) or (2) taking into account the volume of the cell. Analogously, (Fig. 3b) for  $c_{\text{TU}} = 0.5 \text{ mM}$  and  $\eta_a = 0.15 \text{ V}$  ( $I = 6 \mu\text{A}$ ), the charge of the anodic film after  $t_a = 2040 \text{ s}$ , is smaller than that predicted for the complete electro-oxidation of TU. Therefore, the micrograph shown in Fig. 3a can be assigned mainly to film I. This film shows a rather open structure consisting mainly of long thin fibers, although skein-like nodules can also be distinguished. These fibrous structures have been reported previously for the same system under open circuit conditions [6].

On the other hand, when  $c_{\text{TU}} = 0.5 \text{ mM}$  and  $\eta_a = 0.04 \text{ V}$ , after  $t_a = 3600 \text{ s}$ , the charge associated with the anodic film exceeds that predicted by reactions (1) and (2). In this case, the morphology of the deposit (Fig. 4a) changes from the fibrous structure of film I to that of a film consisting of irregular islands with some branching. Otherwise, for  $c_{\text{TU}} = 0.01 \text{ mM}$ , the morphology of the deposit after  $t_a = 3600 \text{ s}$  shows that the topmost part of the dried film is largely inhomogeneous and consists of randomly distributed patches. In this case, the electro-oxidation charge largely exceeds that expected from reactions (1) and (2). Then, film II and  $\text{Cu}^{2+}$  ions in solution are formed. The formation of film II is accompanied by pitting of the copper anode (Fig. 5a). Copper pitting observation can be enhanced after partially dis-

solving the anodic film in aqueous nitric acid (Fig. 5b). Pits surrounded by an annulus of anodic film forming products, and partially filled with the same material, are also observed.

### 3.3. Sequential lateral imaging of the copper/solution profile

No film formation, at least for our sequential lateral imaging scale, could be observed for copper electro-dissolution in aqueous 0.5 mM TU + 0.5 M sulphuric acid in the range  $-0.1 \leq \eta_a \leq 0$  V for  $t_a < 3000$  s. In this potential range the formation of either TU or FDS adsorbates with coverages up to a few monolayers should be expected [7]. Otherwise, in the range  $0 \leq \eta_a \leq 0.07$  V, TU electro-oxidation to FDS, copper electro-dissolution as Cu(I) complexes and the formation of film I can be observed. Film I starts to be formed at the corners of the anode and it takes some time to cover the entire surface. In this case, the average film thickness  $\langle h \rangle$  increases and seemingly the film itself becomes denser as  $t_a$  is increased. For  $\eta_a > 0.07$  V, film I gradu-

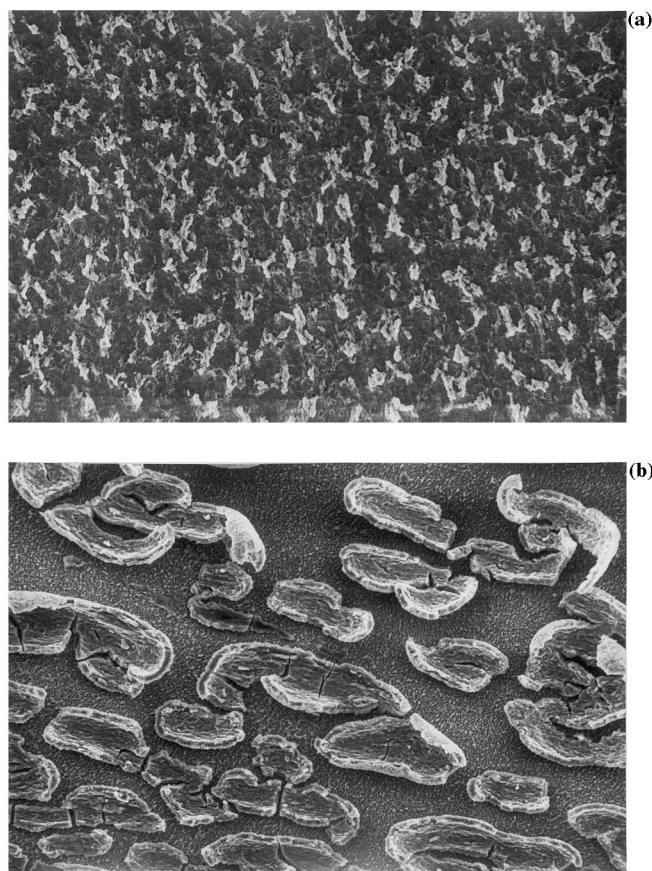


Fig. 4. SEM micrographs of anodic films formed on copper from  $x$  mM TU + 0.5 M sulphuric acid at  $\eta_a = 0.15$  V and  $t_a = 3600$  s. (a)  $x = 0.5$  mM,  $250 \times$ . (b)  $x = 0.01$  mM,  $1000 \times$ .

ally turns into film II which appears as a dark residue mainly consisting of copper sulphide species. Conversely, from the relative image darkness, it can be concluded that films formed for  $\eta_a > 0.15$  V and  $t_a > 60$  s, become entirely uniform right from the very beginning, show no branching, and are slightly brownish.

Sequential lateral images of a copper anode, held at  $\eta_a = 0.15$  V in 0.5 mM TU + 0.5 M sulphuric acid, are shown in Fig. 6. The interface between the lower dark region and the lighter region above it (indicated by arrows in the images) corresponds to the copper anode profile. Film I starts to be formed with an irregular profile at the upper edge of the anode in contact with the solution. It continues growing as an irregular profile for  $t_a > 690$  s. In the range  $1860 \leq t_a \leq 7000$  s, as copper electro-dissolution proceeds, the roughness of the copper surface increases steadily, and film I becomes higher. Initially, the film appears as an inhomogeneous cloud with an irregular growth front. Later, the growth front smoothes out until TU and FDS in the solution are depleted. At this stage a dark layer (film II) on top of the anodic film I is observed. This leads to a net stratification of the anodic film consisting of grey and black alternate layers almost parallel to the edge of the

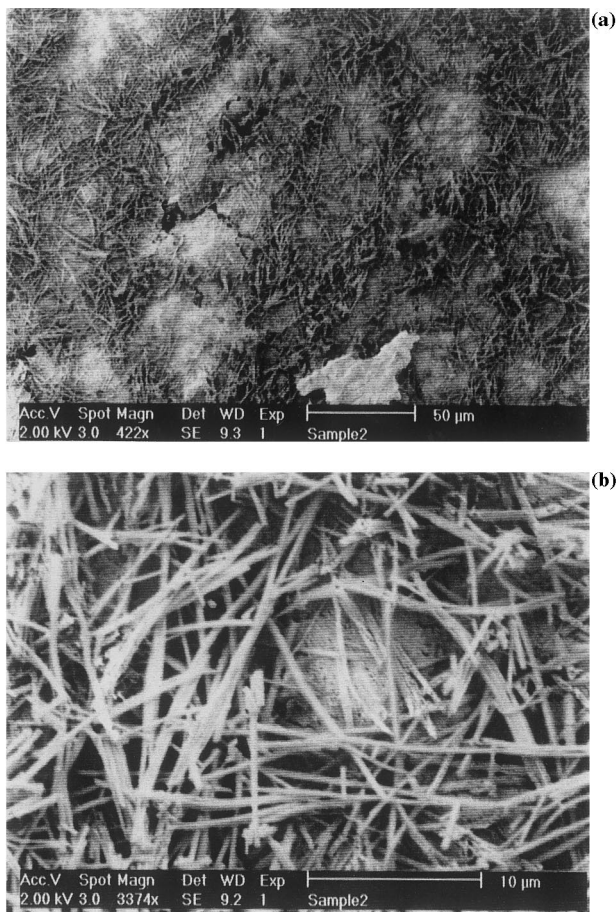


Fig. 3. SEM micrographs of anodic films formed on copper from 0.5 mM TU + 0.5 M sulphuric acid: (a)  $\eta_a = 0.04$  V,  $t_a = 8100$  s; (b)  $\eta_a = 0.15$  V,  $t_a = 2040$  s.

anode. Stratification would suggest that for  $E > 0.07$  V long-lasting oscillating phenomena are probably involved in the formation of the global anodic film.

Sequential photographs of copper anodisation in aqueous 0.5 mM TU + 0.5 M sulphuric acid, at  $\eta_a = 0.26$  V in the range  $60 \leq t_a \leq 300$  s (Fig. 7), show the formation of a more uniform and seemingly denser film as compared to that produced at  $\eta_a = 0.15$  V (Fig. 6). The height of this film grows rather rapidly and stratification appears at a much shorter time, as expected for faster electrodecomposition of Cu(I)–TU complexes, and a higher copper electrodisso- lution rate as soluble Cu(II) ions. The latter reaction probably contributes to the formation of an external amount of anodic copper sludge that also becomes a part of film II.

Anodic films were also produced from aqueous 0.01 and 10 mM TU + 0.5 M sulphuric acid (Figs. 8 and 9). Sequential lateral imaging shows that at  $\eta_a = 0.15$  V the film is rather thin. However, in agreement with the reaction pathway described in Part I [1], the quasi-steady state value of  $\langle h \rangle$  is reached sooner in the 10 mM TU solution than in the 0.5 mM TU solution. From the sequential lateral imaging and solution absorption spectra [1], one can infer that the very beginning of copper electrodisso- lution leads mainly to soluble Cu(I)–TU complex ions rather than to massive anodic film formation. Later, when a certain critical value of  $t_a$  that increases with decreasing  $c_{TU}$  is exceeded, the formation of soluble Cu(II) can be detected.

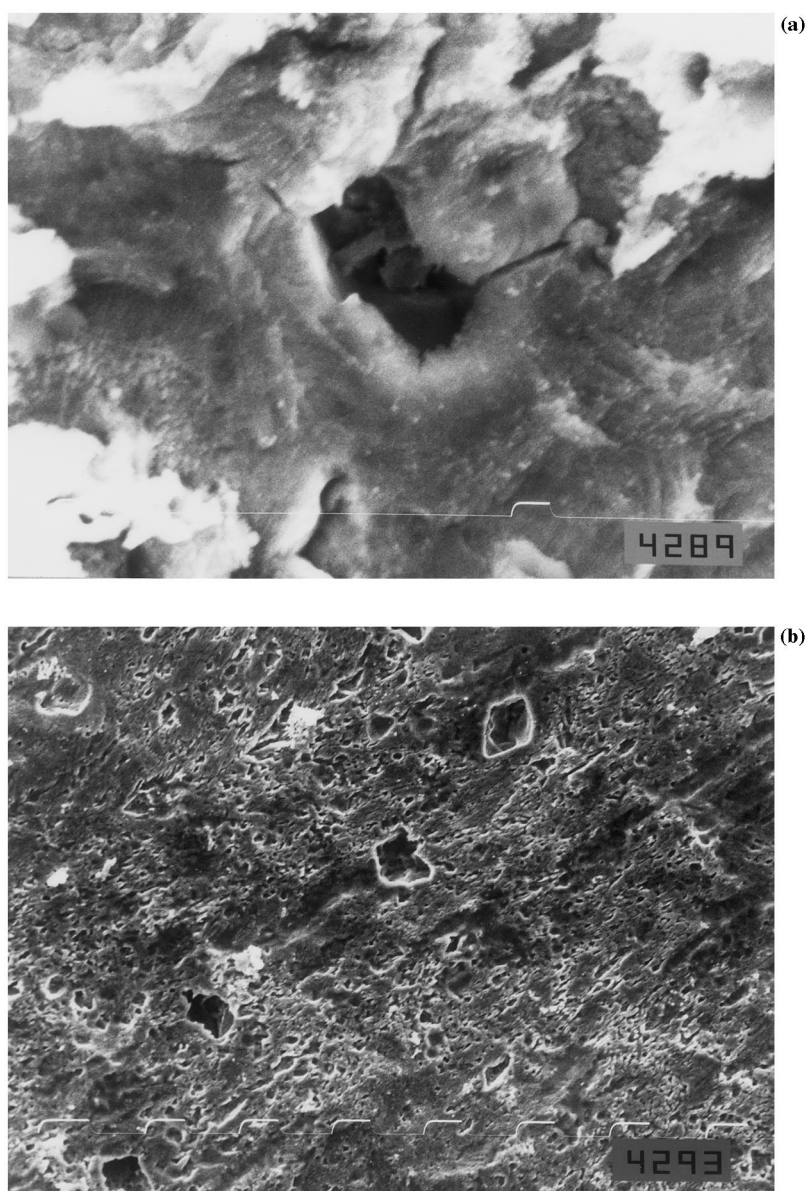


Fig. 5. (a) SEM micrograph of pits formed during the anodisation of copper in 0.01 mM TU + 0.5 M sulphuric acid for  $\eta_a = 0.15$  V and  $t_a = 3600$  s  $7500 \times$ . (b) SEM micrograph resulting after chemical etching with aqueous sulphuric acid + nitric acid mixture  $1500 \times$ .

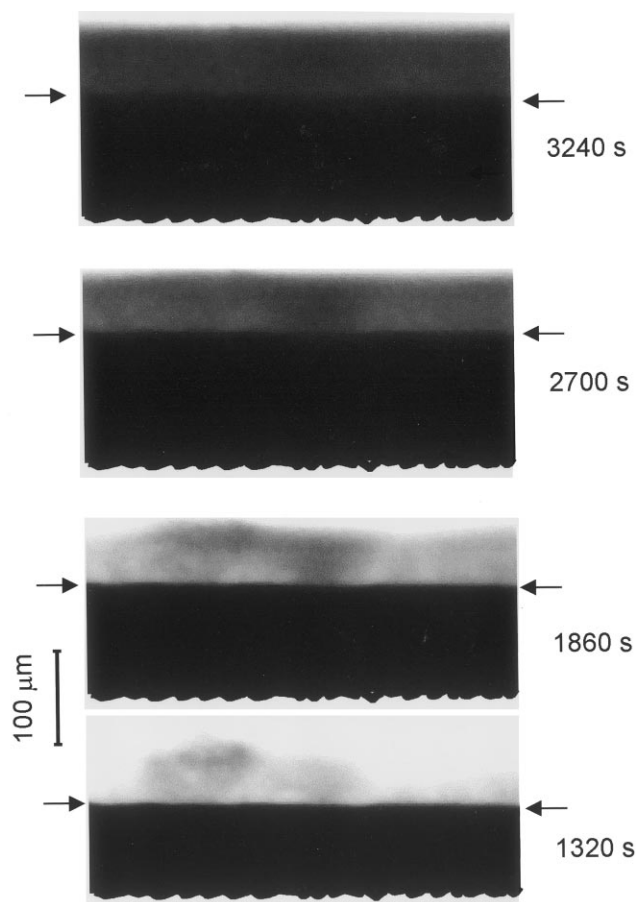


Fig. 6. Sequential lateral imaging of the copper anode|solution interface at  $\eta_a = 0.15$  V in aqueous 0.5 mM TU + 0.5 M sulphuric acid. The arrows indicate the copper anode profile.

For  $\eta_a = 0.04$  V, due to the sensitivity of the experimental technique, no anodic film could be observed in 0.01 mM TU solution, while in 10 mM TU solution only a very thin layer of film I, which attains a steady  $\langle h \rangle$  value, is formed. This fact is consistent with competitive processes involving the simultaneous formation and chemical dissolution of film I at high  $c_{\text{TU}}$  [1]. In this case, one can also observe that copper electrodisso- lution implies an increase in roughness at the anode edge. The roughness increase of the anode can be seen better in diluted TU-containing solutions due to the higher contrast of the various phases in the images. In this case, at  $\eta_a = 0.15$  V, the formation of sulphide residues from Cu(I)–TU electrodecomposition assists the localised corrosion of copper.

It should be noted that for the electrochemical cell used in our work, convective effects contribute to the kinetics of the electrochemical reaction [8]. However, when the density of the solution at the electrode|solution interface decreases upwards, the flow past a flat horizontal plate is stable [9]. This leads to a stable density stratification, as was observed in our experiments for  $\eta_a > 0.15$  V.

### 3.4. Anodic film growth rate

The growth rate of the anodic film can be followed by plotting the values of  $\langle h \rangle$  read from sequential lateral imaging versus  $t_a$ . The shape of these plots depends on  $\eta_a$ ,  $c_{\text{TU}}$  and the range of  $t_a$ .

#### 3.4.1. Influence of potential

From runs made at  $\eta_a = 0.04$  V and  $c_{\text{TU}} = 0.5$  mM (Fig. 10), the  $\langle h \rangle$  versus  $t_a$  plot exhibits four regions. The first region, related to the formation of film I, starts after an induction time ( $t_i$ ) of around 750 s, and for  $750 \leq t_a \leq 1800$  s and  $\langle h \rangle < 110$   $\mu\text{m}$ , it follows a parabolic law (Fig. 10, dotted line). From the initial slope of the  $\langle h \rangle$  versus  $t_a$  plot, the initial growth rate of film I is  $0.1$   $\mu\text{m s}^{-1}$ . The second region extends in the range  $1800 \leq t_a \leq 3300$  s and fits a linear  $\langle h \rangle$  versus  $t_a$  relationship with a growth rate for film II equal to  $0.014$   $\mu\text{m s}^{-1}$ . The third region, in the range  $3500 \leq t_a \leq 4500$  s, shows a fast decrease in  $\langle h \rangle$  with  $t_a$  due to the partial detachment of the film produced by the commencement of copper pitting. Finally, for  $t_a > 4500$  s,  $\langle h \rangle$  tends to reach a steady value.

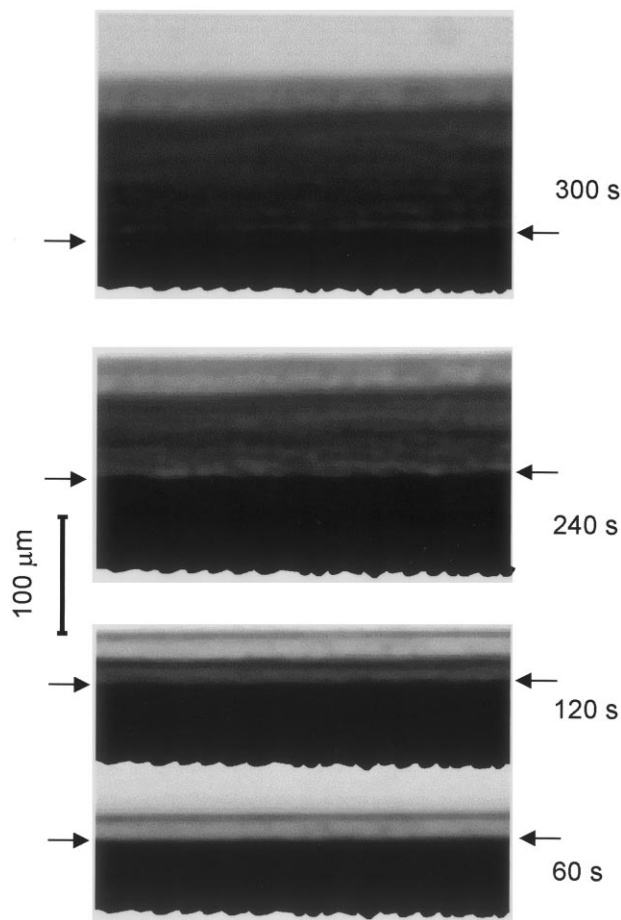


Fig. 7. Sequential lateral imaging of the copper anode|solution interface at  $\eta_a = 0.26$  V in aqueous 0.5 mM TU + 0.5 M sulphuric acid. The arrows indicate the copper anode profile.

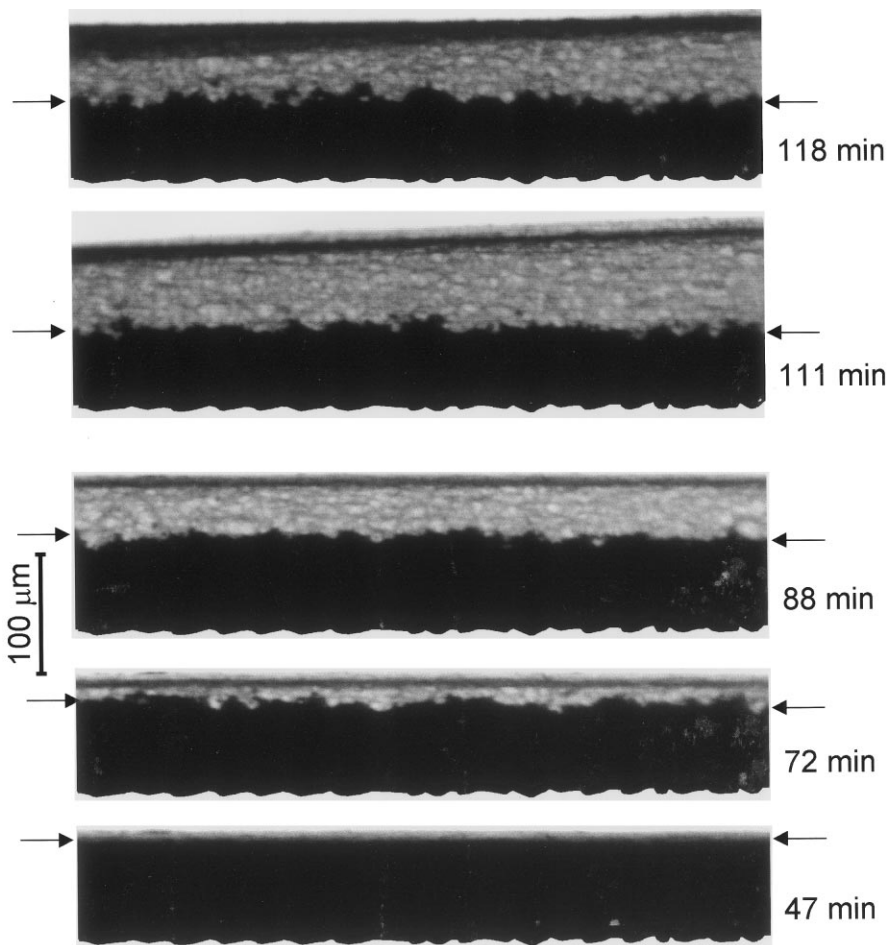


Fig. 8. Sequential lateral imaging of the copper anode | solution interface at  $\eta_a = 0.15$  V in 0.01 mM TU + 0.5 M sulphuric acid.

For  $\eta_a = 0.15$  V and  $c_{\text{TU}} = 0.5$  mM, for  $t_a < 2500$  s and  $\langle h \rangle < 47$   $\mu\text{m}$ , a parabolic relationship between  $\langle h \rangle$  and  $t_a$  after  $t_i \approx 300$  s, was found. In this case, from the initial slope of the linear plot, the growth rate of film I was close to  $0.1$   $\mu\text{m s}^{-1}$ . For the range  $2500 \leq t_a \leq 5000$  s, a linear  $\langle h \rangle$  versus  $t_a$  plot was also obtained. The growth rate of film II was almost the same as that derived for  $\eta_a = 0.04$  V.

Otherwise, from runs made at  $\eta_a = 0.26$  V and  $c_{\text{TU}} = 0.5$  mM, only the linear  $\langle h \rangle$  versus  $t_a$  plot is obtained (Fig. 11). In this case,  $t_i \approx 9$  s and the growth rate of film II is  $0.45$   $\mu\text{m s}^{-1}$ .

These experiments show that at low  $\eta_a$ , i.e. in the potential range where reactions (1) and (2) predominate, the formation of film I occurs in the time range  $t_i \leq t_a \leq t_{c,2}$ , where  $t_{c,2}$  denotes the anodisation time when reactions (1) and (2) come to an end. The value of  $t_{c,2}$  depends on both the reaction rate determined by  $\eta_a$  and  $c_{\text{TU}}$ . In the low  $\eta_a$  range, film I is first formed and later electro-oxidised to film II. In these cases, the growths of film I and film II appear as successive processes and their growth rates are almost  $\eta_a$  independent.

At higher  $\eta_a$ , the formation of film II occurs in the range  $t_i \leq t_a \leq t_{c,3}$ , where  $t_{c,3}$  is the time associated with the full conversion of TU-containing species into film II. This process occurs simultaneously with the electro-dissolution of copper as  $\text{Cu}^{2+}$  ions. The rate of the simultaneous electrochemical reactions leading to film

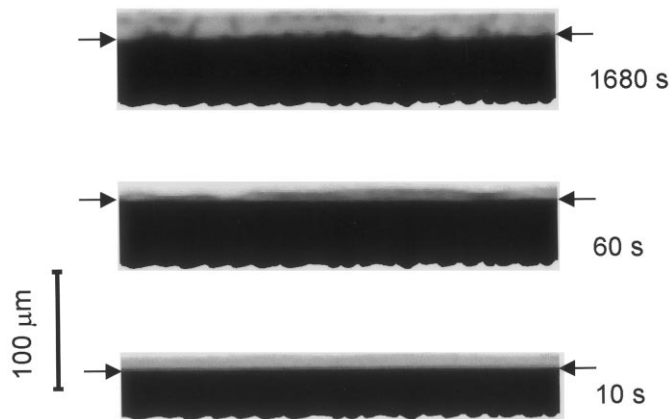


Fig. 9. Sequential lateral imaging of the copper anode | solution interface at  $\eta_a = 0.15$  V in 10.0 mM TU + 0.5 M sulphuric acid.

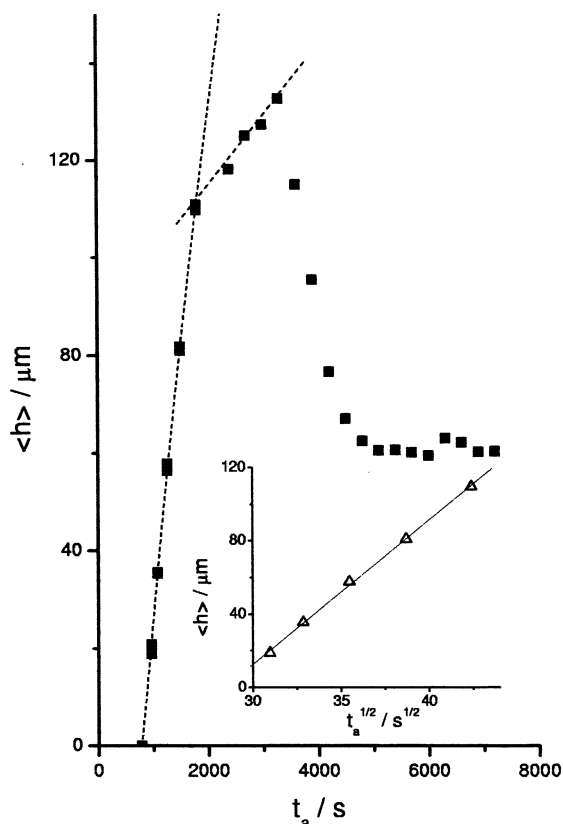


Fig. 10. Average film thickness versus anodisation time plot. Dotted and dashed traces indicate the parabolic (film I) and linear (film II) growth laws, respectively.  $\eta_a = 0.04$  V; aqueous 0.5 mM TU + 0.5 M sulphuric acid.

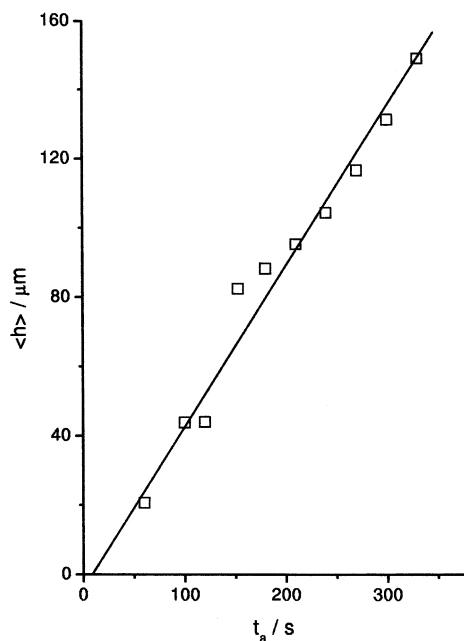


Fig. 11. Linear growth law for film II.  $\eta_a = 0.26$  V; aqueous 0.5 mM TU + 0.5 M sulphuric acid.

II increases with  $\eta_a$ , as expected for an electrochemical reaction under activation control. The electrochemical dissolution of copper as soluble Cu(II) ions, influenced by the presence of film II, occurs as a single process for  $t_a > t_{c,3}$ .

### 3.4.2. Influence of TU concentration

For low  $c_{\text{TU}}$ , i.e.  $c_{\text{TU}} = 0.01$  mM and  $\eta_a = 0.15$  V, the  $\langle h \rangle$  versus  $t_a$  plot (Fig. 12) exhibits the same features as those already described for  $c_{\text{TU}} = 0.5$  mM and  $\eta_a = 0.04$  V (Fig. 10). The first region, for  $t_a < 3500$  s, corresponds to the accumulation of film I up to a maximum value of  $\langle h \rangle$  of about 10  $\mu\text{m}$ . The average growth rate of film I is  $1.6 \times 10^{-3}$   $\mu\text{m s}^{-1}$ , i.e. about fifty times lower than that found for  $c_{\text{TU}} = 0.5$  mM at the same  $\eta_a$ . The growth rate of this film fits a parabolic law after  $t_i \approx 5$  s. Conversely, for the range  $3500 \leq t_a \leq 6000$  s,  $\langle h \rangle$  increases almost linearly with  $t_a$ . In this case, the rate of formation of film II is  $0.046$   $\mu\text{m s}^{-1}$ . The extrapolation of this line to  $\langle h \rangle = 0$  allowed us to estimate the time ( $t_a \approx 3600$  s) for the commencement of film II formation.

The preceding results indicate that the initial ( $t_a \rightarrow 0$ ) rate of formation of film I depends almost linearly on  $c_{\text{TU}}$ . Conversely, as  $c_{\text{TU}}$  decreases, the growth rate of film II increases. This fact is not surprising if one considers that the presence of TU derivatives decreases the rate of copper electrodisolution [1].

### 3.4.3. Displacement rate of the copper front

The rate of copper electrodisolution could also be determined from the displacement of the cop-

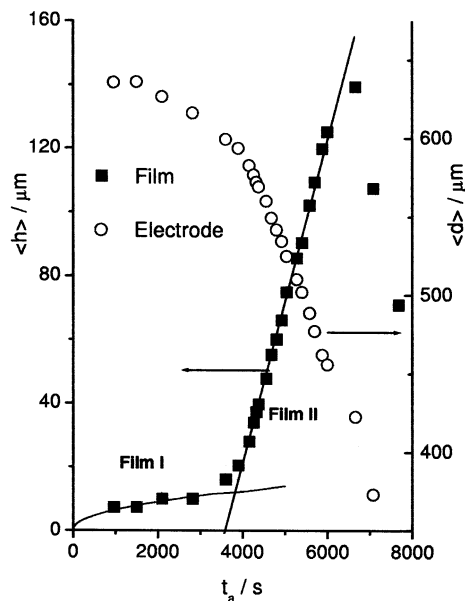


Fig. 12. Dependence of the average film thickness ( $\langle h \rangle$ ) and copper electrode depth ( $\langle d \rangle$ ) on  $t_a$ . Full traces show the parabolic and linear growth law, respectively.  $\eta_a = 0.15$  V; aqueous 0.01 mM TU + 0.5 M sulphuric acid.



per|solution profile from in situ sequential images using the Faraday law and further considering a 100% yield for Cu(I) formation in the presence of TU. In this case, for  $t_a < 4000$  s, the  $\langle d \rangle$  versus  $t_a$  plot (Fig. 12) shows a slow almost linear displacement of the copper front at the rate of  $0.018 \mu\text{m s}^{-1}$ . Subsequently, for  $t_a > 4000$  s, a second linear region with the slope  $0.095 \mu\text{m s}^{-1}$  is found. On the other hand, for  $t_a > 3500$  s, the formation of Cu(II) soluble species can be detected, as indicated in Part I [1].

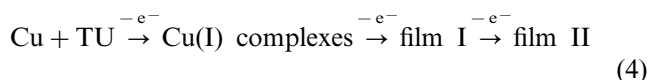
It is interesting to note that the rate of copper electrodisolution depends on whether it occurs simultaneously with the formation of film I or film II. For  $t_a > 4000$  s, the rupture of this film assists the localised electrodisolution of copper as soluble Cu(II) ions.

#### 4. Discussion

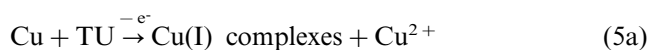
Data have to be analysed and discussed considering the influence of  $\eta_a$ ,  $c_{\text{TU}}$  and  $t_a$  on the faradic yield of different products from batch electrochemical reactions in which several products can be formed. Therefore, the formation of each product can be ascribed to a certain critical anodisation time, which would depend on  $c_{\text{TU}}$  and the charge passed through the cell. Thus, in our case, at least three critical anodisation times can be distinguished, i.e.  $t_{c,1} = t_i$ , which is defined as the induction time for the appearance of film I;  $t_{c,2}$ , related to the full electrodecomposition of FDS and Cu(I)–TU complexes, including film I, into species forming film II; and finally  $t_{c,3}$  which indicates the rupture of film II leading to copper pitting.

Experimental data including SEM micrographs (Figs. 3–5) showed that film I is of heterogeneous nature with fibrous and particulate material dispersed in the anode|solution interface. This material is electro-oxidised further to heterogeneous film II via a complex process. The likely reaction pathway yielding film I was discussed extensively in Part I [1].

At low  $\eta_a$ , neglecting chemical decomposition side reactions, the formation of films I and II can be mainly described by a formalism of consecutive electrochemical oxidation steps



Otherwise, at high  $\eta_a$ , the formation of film II proceeds via a complex reaction pathway involving alternative reactions for the formation of film II such as



where the relative contribution of reactions (5a) and (5b) to reaction (5c) decreases as  $\eta_a$  increases, because the  $\text{Cu(TU)}_{\text{ad}}^+$  species involved in the anodic reaction (2) would react preferentially via reaction (5c). The complex reaction pathway (5a)–(5c) can explain qualitatively the growth kinetics of film I and II described already.

The polarisation curve (Fig. 2) shows that the global anodic reaction is associated with the tendency to a tapered anodic current for  $\eta_a > 0.2$  V, which is due to additional local resistance produced by the anodic film, particularly film II consisting of a mixture of sulphur, copper sulphide and copper [1]. The presence of these films has considerable influence on the kinetics of copper electrodisolution as was referred to in Part I [1].

##### 4.1. Growth kinetics of film I

Film I results from reaction (2) when  $x = 4$  and  $y = 7$  [1]. In all cases an induction time  $t_i = t_{c,1}$ , related to the initiation of the anodic film I growth, can be determined from the  $\langle h \rangle$  versus  $t_a$  plots. For  $t_{c,1} \leq t_a \leq t_{c,2}$ , the growth of film I fits a linear  $\langle h \rangle$  versus  $t_a^{1/2}$  plot (Fig. 10). The value of  $t_{c,1}$  approaches the time that might be expected for the complete electro-oxidation of TU to FDS present in the volume of the 2D cell.

In principle, a parabolic growth law can be explained by simple diffusion kinetics, considering a linear chemical potential gradient of diffusing species acting as the driving force [10]. Thus, from the integration of Fick's first law for a unidirectional transport process, it results in

$$\langle h \rangle = \left( \frac{2D_i}{K} \right)^{1/2} (c_1 - c_0)^{1/2} t_a^{1/2} \quad (6)$$

where  $D_i$  is the diffusion coefficient of the  $i$ th species,  $K$  is a proportionality constant relating concentration and thickness, i.e. a parameter related to the apparent density of the film, and  $c_1$  and  $c_0$  are the concentrations of  $i$ th species at an upper plane and a lower plane related to the moving fronts of the anodic film. As the values of  $c_1$  and  $c_0$  are independent of the thickness, the concentration gradient is inversely proportional to  $\langle h \rangle$ .

As predicted by Eq. (6), a linear  $\langle h \rangle$  versus  $t_a^{1/2}$  plot is obtained for the time range  $t_{c,1} \leq t_a \leq t_{c,2}$ . For  $\eta_a = 0.04$  V and  $c_{\text{TU}} = 0.5$  mM, the slope of this plot  $\Delta\langle h \rangle / \Delta t_a^{1/2} = 7.9 \times 10^{-4} \text{ cm s}^{-1/2}$  (Fig. 10, inset). Considering this, for the simple model,  $c_1 = 0.5$  mM and  $c_0 = 0$  and  $D_i \approx 10^{-6} \text{ cm}^2 \text{ s}^{-1}$  [11–13], it results in  $K = 1.6 \times 10^{-6} \text{ mol cm}^{-3}$ , a figure that is consistent with the open structure of the anodic film. Therefore, the rate of formation of film I is determined by the diffusion of TU into growing film I. In this case, TU molecules are required for copper ion detachment from the surface as  $[\text{Cu}_x(\text{TU})_y]^{x+}$  ions, at the copper anode|film I interface. The possibility that the diffusion

of  $[\text{Cu}_x(\text{TU})_y]^{x+}$  ions into film I might be rate determining appears to be unlikely because it would imply the unlikely situation that  $c_1 \rightarrow 0$  and that  $c_0$  reaches a maximum value at the lower moving front. This would contradict the large faradic efficiency for copper electro-dissolution and the way the profiles of the lower and upper interface change during the process.

#### 4.1.1. Growth kinetics of film II

The formation of film II from film I occurs in the range  $t_{c,2} \leq t_a \leq t_{c,3}$  by electrodecomposition of Cu(I)–TU complexes yielding sulphide species, aqueous Cu(II) ions, Cu(0) and CN-containing adsorbed residues, as concluded from XPS data of solid products, and the presence of Cu(II) ions in solution [1].

The formation of film II is accompanied by a remarkable change in the displacement rate of the copper front (Fig. 12). The ratio of the slopes obtained from the  $\langle d \rangle$  versus  $t_a$  plot for  $t_{c,1} \leq t_a \leq t_{c,2}$  and  $t_{c,2} \leq t_a \leq t_{c,3}$  is close to 1/5. This figure approaches the charge ratio per mole of reacting species for copper electro-dissolution as Cu(I)–TU complexes, and that for copper electro-oxidation of ionic Cu(II) ions plus the charge involved in the film I  $\rightarrow$  film II electro-oxidation reaction, i.e. the occurrence of reaction (2) for  $t_a < t_{c,2}$ , and the formation of aqueous Cu(II) ions and the simultaneous electrodecomposition of Cu(I)–TU complexes into copper sulphide, CN adsorbates and protons for  $t_a < t_{c,3}$ . The electrical conducting properties of film II would be comparable to those of S-containing anodic layers on copper [14–16]. The formation of aqueous Cu(II) ions at the interface might also contribute to the appearance of Cu(0) in the film via the disproportionation reaction  $2\text{Cu(I)} \rightarrow \text{Cu(0)} + \text{Cu(II)}$ . For  $t_a > t_{c,2}$ , the growth of film II results in a film thickness increasing linearly with  $t_a$ , in the range 3600–6000 s (Fig. 12). Film II, as seen by in situ transversal imaging, appears as a low apparent density film. The linear growth of film II means that the flux of reacting species and products is directly determined by the rate of the complex electrochemical process at the copper surface, which is interfered with by anodic residues.

When the whole amount of Cu(I)–TU complexes is electrodecomposed into film II ( $t_a > t_{c,3}$ ), the electro-dissolution of copper as soluble Cu(II) ions is influenced strongly by the presence of film II.

#### 4.1.2. Localised corrosion of copper

Film II behaves as a barrier to copper electro-dissolution to Cu(II) soluble ions (reaction (3)). When  $t_a > t_{c,3}$ , the rupture of film II contributes to the localised corrosion of copper in TU-containing 0.5 M sulphuric acid solutions (Fig. 5). This process resembles that which has been reported for the same metal in solution containing sodium sulphide [14–16]. The formation of a complex copper sulphide layer at potentials slightly

exceeding the reversible Cu/Cu<sub>2</sub>S electrode potential takes place first via a reaction which is very similar to that for the chemical sulphidisation of copper [15]. This copper sulphide layer has been described as a non-stoichiometric layer approaching the stoichiometry of Cu<sub>2</sub>S at the inner layer, and that of CuS at the outer layer. As the potential is further increased, the rupture of the copper sulphide layer occurs leading to localised corrosion of copper promoted by the presence of sulphide [14–16].

## 5. Conclusions

- The sequential in situ imaging of anodic films and copper anode profiles using a 2D cell allowed us to determine the evolution of the copper|film and film|solution profiles and their dependence on the TU concentration in the solution.
- In batch experiments at  $\eta_a$  and  $c_{\text{TU}}$ , different ranges of  $t_a$  that are comprised between critical times are associated with the predominance of a particular electrochemical reaction, i.e. the formation of soluble Cu(I)–TU complexes for  $t_i \leq t_a \leq t_{c,1}$ , and the appearance of film I for  $t_{c,1} \leq t_a \leq t_{c,2}$ . The formation of film II and Cu(II) ions in solution takes place for  $t_{c,2} \leq t_a \leq t_{c,3}$ . Finally, copper pitting occurs for  $t_a > t_{c,3}$ .
- Film I consists of a Cu(I)–TU insoluble complex and is obtained after a certain induction time  $t_i$ . Film II, for  $\eta_a > 0.07$  V, appears as a heterogeneous film mainly constituted by copper sulphide species. These films can be selectively produced by properly adjusting the applied potential, TU concentration in the solution and anodisation time. The transition from film I to film II occurs for  $t_a > t_{c,1}$ .
- The growth kinetics of each anodic film were determined from the average film height growth ( $\langle h \rangle$ ) measured from sequential in situ images. The growth kinetics of film I fit a parabolic rate law, whereas the growth kinetics of film II approach a linear  $\langle h \rangle$  versus  $t_a$  relationship.
- The growth kinetics of film I are determined by the rate of mass transport of TU from the solution towards the anode surface, whereas the growth rate of film II is likely to be determined by the anodic surface reaction at the copper anode.

## Acknowledgements

This work was financially supported by the Consejo Nacional de Investigaciones Científicas y Técnicas (CONICET) (PIP 4376) and Agencia Nacional de Promoción Científica y Tecnológica (PICT 98 06-03251) of

Argentina and the Comisión de Investigaciones Científicas de la Provincia de Buenos Aires (CIC). A.S.M.A.H. thanks the Third World Academy of Science (TWAS) and CONICET for the fellowship granted. The help for the SEM examination provided by Srabani Banarjee of the CISM, Ohio State University is gratefully acknowledged.

## References

- [1] A.E. Bolzán, A.S.M.A. Haseeb, P.L. Schilardi, R.C.V. Piatti, R.C. Salvarezza, A.J. Arvia, *J. Electroanal. Chem.* 500 (2001) 533.
- [2] D.K.Y. Wong, B.A.W. Collier, D.R. MacFarlane, *Electrochim. Acta* 38 (1993) 2121.
- [3] A.E. Bolzán, I.B. Wakenge, R.C.V. Piatti, R.C. Salvarezza, A.J. Arvia, submitted.
- [4] P.L. Schilardi, R.C.V. Piatti, A.E. Bolzán, R.C. Salvarezza, A.J. Arvia, in preparation.
- [5] E.O. Piro, R.C.V. Piatti, A.E. Bolzán, R.C. Salvarezza, A.J. Arvia, *Acta Crystallogr., Sect. B* (in press).
- [6] A. Hernández Creus, R.M. Souto, S. González, M.M. Laz, R.C. Salvarezza, A.J. Arvia, *Appl. Surf. Sci.* 81 (1994) 387.
- [7] O. Azzaroni, B. Blum, R.C. Salvarezza, A.J. Arvia, *J. Phys. Chem. B Lett.* 104 (2000) 1395.
- [8] P.L. Schilardi, O. Azzaroni, R.C. Salvarezza, A.J. Arvia, *Phys. Rev. B* 59 (1999) 4638.
- [9] H. Schlichting, *Boundary Layer Theory*, McGraw Hill, New York, 1968.
- [10] M.A. Genshaw, in: E. Gileadi (Ed.), *Electrosorption*, Plenum, New York, 1967 Ch. 4.
- [11] J. Kirchenerová, W.C. Purdy, *Anal. Chim. Acta* 123 (1981) 83.
- [12] M. Alodan, W. Smyrl, *Electrochim. Acta* 44 (1998) 299.
- [13] A.E. Bolzán, I.B. Wakenge, R.C. Salvarezza, A.J. Arvia, *J. Electroanal. Chem.* 475 (1999) 181.
- [14] T.P. Hoar, A.J.P. Tucker, *J. Inst. Met.* 81 (1952) 665.
- [15] E.M. Kahiry, N.A. Darwish, *Corros. Sci.* 13 (1973) 141.
- [16] D. Vázquez Moll, M.R.G. de Chialvo, R.C. Salvarezza, A.J. Arvia, *Electrochim. Acta* 30 (1985) 1011.